Limnol. Oceanogr., 59(5), 2014, 1621–1636

doi:10.4319/lo.2014.59.5.1621

Modern seasonality in Lake Challa (Kenya/Tanzania) and its sedimentary documentation in recent lake sediments

Christian Wolff,[1,2,3,*] Iris Kristen-Jenny,[1] Georg Schettler,[1] Birgit Plessen,[1] Hanno Meyer,[4] Peter Dulski,[1] Rudolf Naumann,[1] Achim Brauer,[1] Dirk Verschuren,[5] and Gerald H. Haug[3,6]

[1] Helmholtz Centre Potsdam, German Research Centre for Geosciences, Climate Dynamics and Landscape Evolution, Potsdam, Germany
[2] Institute of Earth and Environmental Science, University of Potsdam, Potsdam, Germany
[3] German Research Foundation, Leibniz Center for Earth Surface Process and Climate Studies, University of Potsdam, Potsdam, Germany
[4] Alfred Wegener Institute, Helmholtz Centre for Polar and Marine Research, Research Unit Potsdam, Potsdam, Germany
[5] Limnology Unit, Department of Biology, Ghent University, Gent, Belgium
[6] Geological Institute, Department of Earth Sciences, Swiss Federal Institute of Technology in Zurich, Zurich, Switzerland

Abstract

From November 2006 to January 2010, a sediment trap that was cleared monthly was deployed in Lake Challa, a deep stratified freshwater lake on the eastern slope of Mt. Kilimanjaro in southern Kenya. Geochemical data from sediment trap samples were compared with a broad range of limnological and meteorological parameters to characterize the effect of single parameters on productivity and sedimentation processes in the crater basin. During the southern hemisphere summer (November–March), when the water temperature is high and the lake is biologically productive (nondiatom algae), calcite predominated in the sediment trap samples. During the "long rain" season (March–May) a small amount of organic matter and lithogenic material caused by rainfall appeared. This was followed by the cool and windy months of the southern hemisphere winter (June–October) when diatoms were the main component, indicating a diatom bloom initiated by improvement of nutrient availability related to upwelling processes. The sediment trap data support the hypothesis that the light–dark lamination couplets, which are abundant in Lake Challa cores, reflect seasonal delivery to the sediments of diatom-rich particulates during the windy months and diatom-poor material during the wet season. However, interannual and spatial variability in upwelling and productivity patterns, as well as El Niño–Southern Oscillation (ENSO)-related rainfall and drought cycles, exert a strong influence on the magnitude and geochemical composition of particle export to the hypolimnion of Lake Challa.

The influence of global warming on freshwater availability in Africa is attracting increasing attention (Cullen et al. 2006; Mölg et al. 2008; Olaka et al. 2010). Annually laminated lacustrine sediments provide potential information about changes in the large-scale atmospheric circulation and associated moisture-balance variation (Gasse et al. 1989; Johnson et al. 2002; Wolff et al. 2011). Paleoclimatic reconstructions on the basis of lake sediments require understanding of the lake's response to the seasonality of environmental parameters, such as temperature and precipitation (Mackay et al. 2005). Monitoring of the modern lake systems provides insight into sediment formation and preservation in the context of seasonal climatic variability (Pilskaln 2004; Bluszcz et al. 2008; Stockhecke et al. 2012). However, the majority of published records on seasonal aspects of lacustrine sediment formation are from temperate region lakes (Ojala et al. 2012). Microfacies and geochemical data extracted from sediment trap and water samples from Lake Challa, a tropical crater lake on the lower eastern flank of Mt. Kilimanjaro, were compared with a broad range of limnological and meteorological parameters to understand the forcing of external factors and the influence of lake internal processes on the formation of seasonal laminae in tropical lake sediment. Our aim is to understand the genesis of the sedimentary record of Lake Challa to provide a reliable mechanistic model for paleoclimatic interpretation of the lake's sediment record and varve formation.

Study site and modern-day climate—Lake Challa (3°19′S, 37°42′E) is a crater lake with steep walls (up to 170 m) on the lower eastern slope of Mt. Kilimanjaro (Fig. 1). Maximum depths varied between 92 m and 98 m in 1999–2010. The lake surface area is approximately 4.5 km^2, and it is ~ 880 m above sea level. The drainage basin is composed of igneous rocks (predominantly trachy-basalts) of the tertiary Kilimanjaro complex (Bear 1955) covered by "calcareous tuffaceous grits," a calcite-cemented tuffaceous breccia (Downie and Wilkinson 1972). This volcanic complex is underlain by metamorphic rocks (predominantly gneisses) that outcrop east and south of Lake Challa to the Indian Ocean coast (Petters 1991). A seismic survey detected a sediment infill of ~ 210 m on the bottom of the crater, which accumulated over ~ 250,000 yr (Moernaut et al. 2010).

Evaporation (1700 mm yr^{-1}) exceeds the annual rainfall onto the surface of the lake (600 mm; Payne 1970). Therefore, the water budget of the lake is mostly controlled by subsurface in- and outflow in which the groundwater input is probably fed by seepage of precipitation falling

* Corresponding author: wolff@geo.uni-potsdam.de

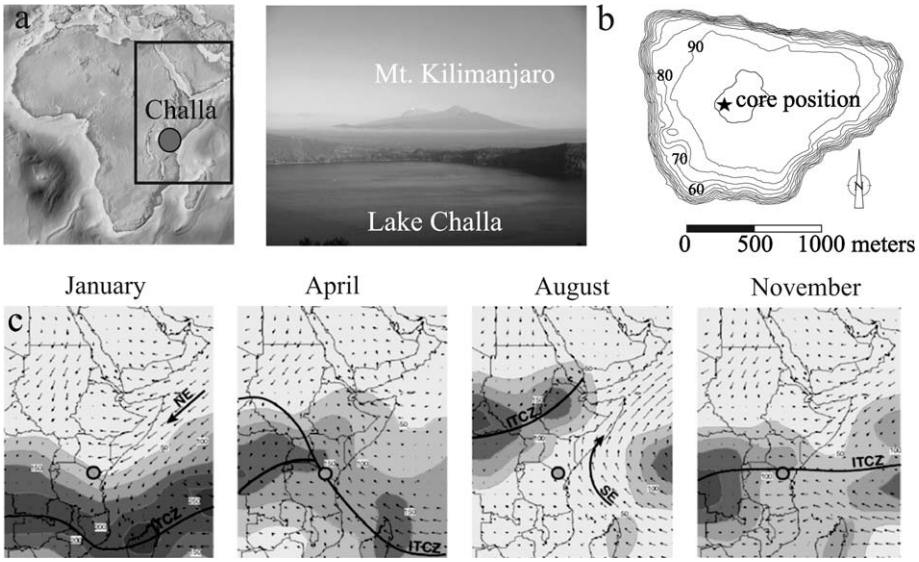

Fig. 1. (a) Location of Lake Challa (3°19′S, 37°42′E) and (b) bathymetric map (depth contours at 10 m intervals (Moernaut et al. 2010). (a) Black outline indicates coverage area shown in (c). (c) Seasonal migration of the ITCZ over Eastern Africa with northeasterly (NE) and southeasterly (SE) trade winds. Monthly precipitation (shading, mm month^{-1}) based on satellite precipitation estimates over ocean areas and rain gauge data over land regions; contours are drawn at 50 mm intervals. Large-scale wind vectors for the 925 hectopascal pressure level indicate wind direction with wind speed proportional to the length of the vectors. Source: http://iridl.ldeo.columbia.edu.

further uphill in the forest zone on the slopes of Mt. Kilimanjaro. Local climate is controlled by the seasonal passage of the Inter-Tropical Convergence Zone (ITCZ; Fig. 1), with rainfall occurring predominantly from October to December and March to May (Fig. 2; Nicholson 2000). These two rainy seasons are referred to as the ''long rains'' (March–May), usually the major rainfall of the year, and the ''short rains'' (October–December), which are more variable. Long rains and short rains presumably respond to changes in Indian Ocean surface-water temperatures and related forcing on atmospheric circulation (Black et al. 2003; Hastenrath et al. 2004). Furthermore, rainfall in East Africa is linked to the El Niño–Southern Oscillation (ENSO), with more rain during El Niño years and severe droughts in La Niña years (Ropelewski and Halpert 1987; Nicholson 2000). Temperatures in the region south of the equator are high during northern hemisphere winter (November–March) and decline by about 4°C during the northern hemisphere summer (June–August). In contrast to temperature, seasonal wind speed variations show the

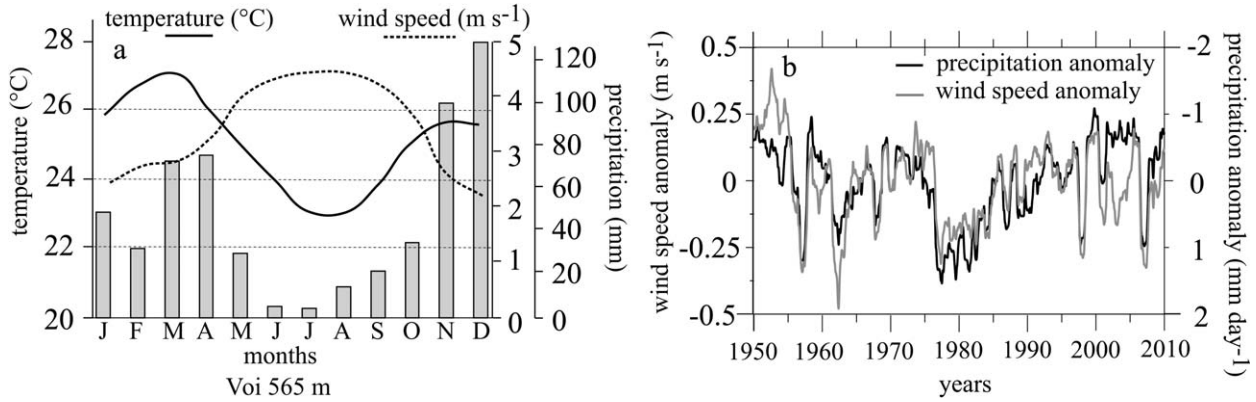

Fig. 2. (a) Meteorological data from Voi, Kenya (~ 100 km east of Lake Challa). Black line, annual temperature trend; bars, monthly rainfall amount; dashed line, monthly wind speed data; source: monthly station data via the Global Climate Perspective System from the National Climatic Data Center by the National Oceanic and Atmospheric Administration (NOAA NCDC GCPS). (b) Comparison between the 13 months running mean of wind speed and negative precipitation anomalies (13 months running mean) indicates the inverse relationship between rainfall and wind speed on interannual timescales in the region around Lake Challa (4°S–3°S, 37°E–38°E); source: National Centers for Environmental Prediction and National Center for Atmospheric Research (NCEP-NCAR) reanalysis dataset (Kalnay et al. 1996).

Table 1. Hydrochemical water profiles from Lake Challa, 23 Aug 2007 (18:00 h) and 28 Nov 2007 (12:00 h). All units mg L^{-1}.

Depth (m)	Na	K	Ca	Mg	Fe	Mn	Sr	Ba	F	Cl	DIC	SO_4	SRP	NPOC	NH_4	NO_3	Si	TDS
23 Aug 2007 (18:00 h)																		
0	19.3	5.8	19.2	21.2	0.008	0.001	0.228	0.006	0.20	9.9	38.4	3.1	<0.005	6.7	<0.025	0.28	20.7	343
5	20.2	6.4	19.8	22.2	0.010	0.003	0.235	0.007	0.27	9.8	38.2	3.2	<0.005	3.9	<0.025	<0.2	20.6	345
10	19.8	6.2	19.6	22.3	0.006	0.002	0.233	0.006	0.31	9.8	38.2	3.4	<0.005	3.0	<0.025	<0.2	20.9	346
15	19.5	6.1	19.5	22.1	0.007	0.001	0.229	0.006	0.30	9.7	38.4	2.8	<0.005	2.8	<0.025	<0.2	20.5	344
20	19.4	5.9	19.4	22.3	0.005	0.001	0.228	0.006	0.27	9.9	37.5	3.2	<0.005	2.8	<0.025	1.53	20.8	341
30	20.0	6.1	20.2	23.3	0.044	0.002	0.236	0.008	0.28	9.8	38.3	3.3	<0.005	1.8	<0.025	2.01	20.6	347
40	19.6	5.8	19.9	23.3	0.006	0.001	0.232	0.006	0.27	9.8	38.8	3.0	<0.005	1.5	<0.025	<0.2	21.1	350
50	19.0	6.1	22.7	22.7	0.032	0.091	0.235	0.009	0.23	9.6	41.9	2.0	0.029	1.5	0.77	2.14	21.6	368
60	19.2	5.9	31.3	23.9	0.070	0.104	0.264	0.010	0.32	9.1	48.0	1.2	0.160	1.6	2.32	0.34	24.9	419
70	18.8	6.2	36.7	23.5	0.065	0.111	0.272	0.011	0.26	9.3	53.0	1.2	0.288	1.8	3.97	0.51	28.4	461
80	18.7	5.7	38.4	24.2	0.070	0.112	0.279	0.011	0.25	8.8	53.8	<0.3	0.325	1.7	4.43	<0.2	28.4	465
28 Nov 2007 (12:00 h)																		
0	22.4	6.7	21.7	22.8	<0.001	0.001	0.256	0.005	0.25	10.3	40.0	2.9	NA	NA	<0.025	<0.2	21.2	362
10	22.2	6.6	21.5	22.7	<0.001	0.001	0.256	0.005	0.31	10.4	40.0	3.2	<0.005	NA	<0.025	<0.2	22.5	366
20	21.4	6.4	21.1	22.3	<0.001	0.001	0.254	0.005	0.31	10.1	39.0	2.6	<0.005	NA	<0.025	<0.2	20.4	351
40	21.0	6.3	22.0	21.9	<0.001	0.006	0.248	0.006	0.28	9.4	39.1	2.9	<0.005	NA	<0.025	<0.2	21.8	356
60	20.8	6.5	33.4	22.3	0.010	0.103	0.284	0.010	0.30	9.2	45.7	1.8	0.138	NA	<0.025	9.3	26.0	414
80	21.8	6.7	21.7	22.9	<0.001	0.002	0.259	0.005	0.31	10.3	40.6	3.1	<0.005	NA	<0.025	<0.2	20.4	362
90*	21.4	7.2	22.5	22.2	<0.001	0.006	0.252	0.006	0.28	9.8	39.9	2.8	<0.005	NA	0.121	<0.2	20.7	358
95	21.8	6.9	22.4	22.6	0.014	0.004	0.256	0.006	0.27	10.3	39.9	2.7	<0.005	NA	<0.025	<0.2	20.7	360

NA, not analyzed; DIC, dissolved inorganic carbon; SRP, soluble reactive phosphorus; NPOC, nonpurgeable dissolved organic carbon; TDS, total dissolved solids; *, average of two water analyses.

Table 2. Chemical composition of local rocks and soils (all collected within 30 km around Lake Challa). Element ratios refer to mass ratios.

Sample description	SiO_2	TiO_2	Al_2O_3	Fe_2O_3	MnO	MgO	CaO	Na_2O	K_2O	P_2O_5	H_2O
Unweathered grits (Challa)	35.94	4.04	9.70	14.21	0.21	8.53	15.93	1.50	0.68	0.93	2.74
Weathered grits (crater rim)	39.93	4.29	10.98	15.46	0.23	8.51	11.03	1.41	2.12	1.14	3.55
Soil on grits (crater rim)	38.13	4.21	10.96	14.04	0.21	8.28	11.34	0.35	1.13	0.84	5.97
Local lava (crater rim)	40.70	3.26	11.10	12.89	0.19	12.20	13.01	1.77	0.71	0.63	2.23
Soil on lava (crater rim)	41.15	4.03	11.70	14.65	0.22	7.22	9.88	1.94	1.83	0.93	3.55
Pumice pieces (crater rim)	39.36	3.32	11.77	13.44	0.20	12.52	13.51	0.57	0.48	0.56	3.18
Soil on pumice (crater rim)	38.30	3.81	11.19	13.52	0.20	10.54	9.80	0.75	0.79	0.64	5.28
Unweathered basalt	44.89	3.77	15.15	14.13	0.19	5.31	8.28	3.29	1.74	0.69	1.79
Unweathered basalt	45.50	3.79	16.10	13.57	0.19	4.56	8.69	3.27	1.53	0.84	1.29
Soil on basalt	40.46	4.32	13.10	17.16	0.24	7.66	8.19	1.74	1.40	0.73	3.11
Soil from Challa	37.20	4.24	16.71	15.82	0.24	3.20	7.16	0.71	1.22	0.71	7.12
Soil from Challa village	41.21	3.97	17.32	15.54	0.25	3.03	4.07	0.21	1.09	0.67	8.28
Sand of pool in ravine*	34.01	4.71	16.09	17.91	0.25	3.26	4.49	0.27	0.81	0.87	9.03
Sandy clay from dry river bed	33.20	5.38	17.62	22.09	0.30	2.78	1.62	0.09	0.25	0.51	10.15
Fsp-rich gneiss (Reata Mt.)	75.42	0.14	12.64	1.74	0.07	0.15	0.86	2.04	5.77	0.03	0.73
Soil on fsp-rich gneiss	60.03	1.59	13.35	6.91	0.11	1.05	2.53	1.90	3.30	0.18	3.06
Banded gneiss (Reata Mt.)	77.33	0.05	12.43	0.70	0.00	0.01	0.60	3.24	4.84	0.02	0.66
Soil on banded gneiss	58.01	1.73	17.18	8.78	0.15	1.00	3.13	2.58	2.15	0.19	3.15
UCC (Rudnick and Gao 2003)		0.64	15.40	2.00	0.10	2.48	3.59	3.27	2.80	0.15	

* Ravine (~ 500 m long) enters Lake Challa in northwest corner of caldera and is, according to information from local people, only active in very wet years; fsp, feldspar; element ratios refer to mass ratios.

inverse pattern, with weak northeasterly trade winds prevailing from November to April and strong southeasterly winds from May to October when the ITCZ is displaced northward.

Methods

Temperature profiles were recorded at 2 h intervals between November 2006 and January 2010 by eight temperature loggers (Minilog, Vemco, Canada) placed (10, 20, 30, 40, 50, 60, 65, 85 m) at a mooring site close to the center of the lake. Water for chemical analyses was sampled along vertical profiles at various depths on 23 August 2007 and 28 November 2007, using a Hydro-Bios Plastic Water Sampler (Niskin type). Water samples (100 mL each) were filtered through 0.2 μm, 25 mm diameter Whatman GD/X polypropylene syringe filters, and 50 mL was acidified with concentrated HNO_3 for analyses of cations and was stored at 4°C until processing. Chemical analyses closely followed Eggermont et al. (2007). Profiles of temperature, pH, conductivity, and dissolved oxygen were measured using a Hydrolab Quanta conductivity, temperature, depth (CTD) profiler and a multiparameter water quality meter (Yellow Springs Instrument Company 600XL-B-D), respectively.

Water samples for stable isotope analyses of oxygen ($\delta^{18}O$) and deuterium (δD) were collected in August and November 2007 from various water depths (0 to 90 m in 10 m steps) and were stored in sealed air-tight polypropylene bottles until analysis at the Alfred Wegner Institute for Marine and Polar Research in Potsdam. A Finnigan Delta-S stable isotope ratio mass spectrometer equipped with two equilibration units was used for the determination of hydrogen and oxygen isotope composition, following Meyer et al. (2000). Analytical precision was better than 0.8‰ for δD and 0.1‰ for $\delta^{18}O$.

In November 2006, a Uwitec (double-funneled 86 mm diameter) sediment trap was installed below the thermocline at 35 m water depth close to the center of the lake (core position Fig. 1) to record seasonal changes in primary production, carbonate precipitation, and deposition of siliciclastics. The trap was emptied and redeployed every ~ 4 weeks, providing 34 monthly samples between December 2006 and January 2010. After settling for a minimum of 24 h and the decanting of superfluous water, samples were stored frozen until further preparation in the GeoForschungsZentrum (GFZ) laboratories in Potsdam, where the solids were separated by filtration (Schleicher & Schnell RC-L 60, 1 μm, 50 mm) and were freeze dried. Major and trace elements of sediment trap materials were analyzed using an inductively coupled plasma atomic emission spectrometer (ICP-AES; Thermo Elemental Cooperation, iCAP 6000 series) after wet decomposition. The digestion of sample aliquots between 1.8 mg and 57.9 mg (depending on the amount of available material) using Merck (Suprapur) acids comprised the following steps: (1) carbonate dissolution and wet oxidation of organic material (HNO_3 [30%], 3 h, 130°C), (2) oxidation of refractory organic compounds ($HClO_4$ [70%], 5 h, 160°C), (3) silicate dissolution (HF [40%], 2 days, 70°C), (4) evaporation of HF and Si-F compounds ($HClO_4$ [70%], 2 h, 210°C), and (5) dissolution in 2 mL HCl and filling to a final volume of 14 mL. Four multielement standards in an acid matrix similar to that of the digestion solutions were prepared for external calibration on the basis of commercial single-element standards of Spex and Merck, respectively. The total carbon (TC) and total organic carbon (TOC) analyses were performed using an elemental analyzer (NC2500 Carlo

Table 2. Extended.

CO_2	S	Ca : Al	K : Al	Si : Al	Ti : Al	Fe : Al	Mn : Al	Mg : Al	Mn : Fe	Al : Fe
4.68	99.09	2.22	0.07	3.27	0.47	1.94	0.03	1.00	0.02	0.52
0.72	99.37	1.36	0.19	3.21	0.44	1.86	0.03	0.88	0.02	1.36
3.99	99.45	1.40	0.10	3.07	0.43	1.69	0.03	0.86	0.02	1.40
0.63	99.33	1.58	0.06	3.24	0.33	1.53	0.03	1.25	0.02	1.58
2.31	99.41	1.14	0.16	3.11	0.39	1.65	0.03	0.70	0.02	1.14
0.54	99.46	1.55	0.04	2.95	0.32	1.51	0.03	1.21	0.02	1.55
4.60	99.42	1.18	0.07	3.02	0.39	1.60	0.03	1.07	0.02	1.18
0.23	99.46	0.74	0.11	2.62	0.28	1.23	0.02	0.40	0.02	0.74
0.15	99.47	0.73	0.10	2.50	0.27	1.11	0.02	0.32	0.02	0.73
1.30	99.42	0.84	0.11	2.73	0.37	1.73	0.03	0.67	0.02	0.84
5.15	99.49	0.58	0.07	1.97	0.29	1.25	0.02	0.22	0.02	0.58
3.83	99.48	0.32	0.06	2.10	0.26	1.19	0.02	0.20	0.02	0.84
7.82	99.52	0.38	0.05	1.87	0.33	1.47	0.02	0.23	0.02	0.68
5.54	99.54	0.12	0.01	1.66	0.35	1.66	0.03	0.18	0.02	0.60
0.15	99.75	0.09	0.46	5.27	0.01	0.18	0.01	0.01	0.05	5.50
5.56	99.57	0.26	0.25	3.97	0.13	0.68	0.01	0.09	0.02	1.46
0.05	99.93	0.07	0.39	5.49	0.00	0.07	0.00	0.00	0.00	13.44
1.49	99.54	0.25	0.13	2.98	0.11	0.68	0.01	0.07	0.02	1.48

Erba). The results were referenced against lab-internal soil standards and a reference sample (urea). Total inorganic carbon (TIC) was determined as the difference between TC and TOC. Saturation indices for calcite, aragonite, and amorphous silica in the water column were calculated using PHREEQC software (Version 2, database: Phreeqc; Parkhurst and Appelo 1999).

Sediment investigations were carried out on a 49 cm long gravity core, taken from the center of the lake. Sedimentary structures were studied under the microscope on thin sections from 10 cm long resin-impregnated blocks (Merkt 1971; Brauer et al. 1999). Sediment components were studied in smear slides, which were prepared with Merck Kaiser's glycerol gelatin for microscopy (melts at 40°C). Scanning electron microscope (SEM) images were performed using a Carl Zeiss Ultra 55 Plus system. Changes in sediment composition and intensities of chemical elements in the top 10 cm of the gravity core (~ last 100 yr) were studied by micro X-ray fluorescence (μXRF) scanning of the sediment, imbedded in a resin-block. Scanning was performed using an EAGLE III XL μXRF spectrometer (Röntgenanalytik) at GFZ, applying 40 kV tube voltage, 300 μA tube current, 123 μm spot size, and 100 μm step size.

Samples of powdered catchment rocks and soils were mixed and fused with Li tetraborate–metaborate flux (FLUXANA, FX-X65). The prepared glass discs were analyzed using wavelength-dispersive XRF spectrometry (Panalytical Axios Advanced XRF spectrometer). Quantification of element concentrations was achieved using calibration curves generated from multiple certified reference samples.

Results

Physical and chemical lake water characteristics—Lake Challa is a tropical hard-water lake with HCO_3 as the dominant anionic component, followed by Cl and SO_4 (Table 1). According to Talling and Talling (1965), this is the dominant (prevailing) type of lake water in Africa. A substantial proportion of the high dissolved inorganic carbon (DIC) inventory of the lake may originate from chemical dissolution of the local calcite-bearing tuffaceous breccia (cf. Table 2; CO_2 contents of unweathered and weathered grit). The DIC : Ca equivalent ratio of the lake water is approximately three times higher than that of fluids derived from carbonate dissolution. This relatively high DIC : Ca may have been generated by inflow of fluids from CO_2-forced chemical silicate weathering and aerobe mineralization of organic matter over time. There is no evidence for active CO_2-rich sublacustrine springs within the lake basin.

Sulfate concentrations in Lake Challa are generally low, and they decrease in the anoxic bottom water (Fig. 3f). Soluble reactive phosphorus (SRP) was not detectable in the upper 40 m of the water column (Fig. 3d,j); it is obviously limiting for phytoplankton in Lake Challa, in particular for diatom blooms, which would be supported by high Si concentration of the lake (Barker et al. 2011).

High concentrations of SRP and NH_4 in deep water (> 40 m water depth; August 2007) probably reflect the release of PO_4 and NH_4 from sedimenting particles and the diffusive reflux of both components across the sediment–water interface under anoxic conditions. In November 2007, seasonal depletion of both ions was due to oxygenation of the deep water (Fig. 3).

Nitrate is very low in the top 20 m (August 2007) to 40 m (November 2007), respectively, where it is probably consumed by primary producers. The presence of NO_3 in 20 m to 30 m and 50 m to 70 m water depth in August 2007 (Fig. 3e; Table 1) and at ~ 60 m in November 2007 reflects microbe-mediated organic matter degradation and nitrification under oxic conditions (Buckles et al. 2013). Oxygen

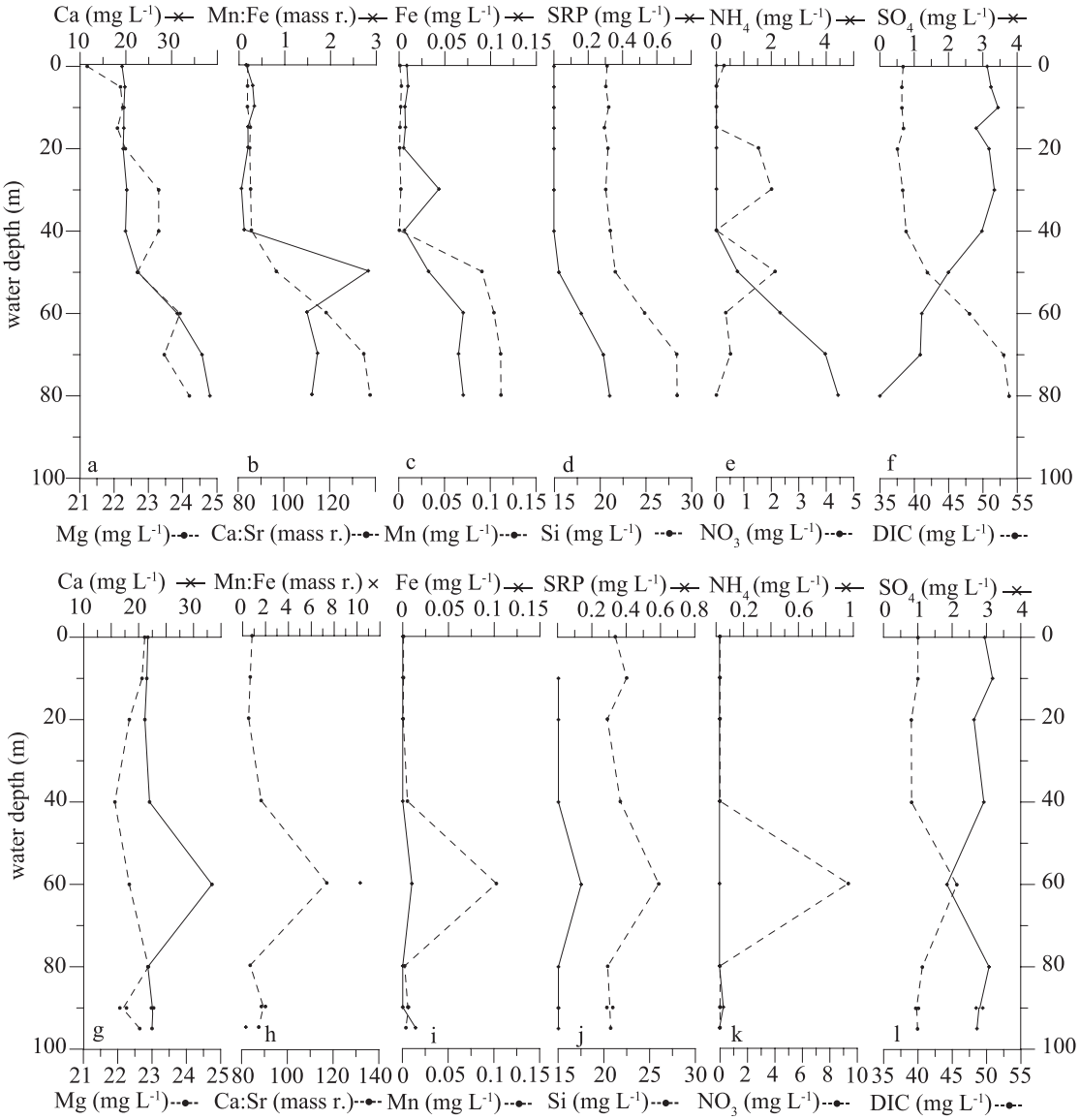

Fig. 3. Selected hydrochemical profiles of chemical lake water characteristics of Lake Challa: (a–f) were recovered on 23 August 2007 (18:00 h), (g–l) were recovered on 28 November 2007 (12:00), 90 m water depth samples are duplicate. For the complete water chemistry data sets *see* Table 1. SRP, soluble reactive phosphorus.

concentrations in water profiles indicate permanent anoxic conditions in the deep water. Moreover, the density contrast along the water column between 40 m and deep water inhibits mixing of the entire water column during weakening of thermal stratification during southern hemisphere winter (Fig. 4a,b,d).

The presence of NO_3 in deep water from August 2007 indicates previous deep-water oxygenation and related nitrifying activity. Furthermore, the combined increase of SO_4 and decrease of total dissolved solids (TDS) between August and November 2007 indicate a short-term overturn event of the water column. Alternatively, the presence of NO_3 and SRP at 60 m in November 2007 could be an indication of groundwater inflow. However, the profiles of inert ions (Na, K, Mg, Cl) do not support this interpretation (Table 1). Notably, the water profile from 23 August 2007 shows increased TDS and electric conductivity (EC) in deep water, which correlates with an increase in Ca and DIC (Table 1). The increase of both components most likely reflects the dissolution of autochthonous calcite and an increase in DIC due to microbe-mediated mineralization of organic matter. Undersaturation of calcite in deep water supports this interpretation.

In general, Si concentrations are high in Lake Challa ($>$ 20 mg L^{-1}, Table 1). Under stratified conditions in August 2007, higher Si concentrations in the hypolimnion (Fig. 3) reflect diatom dissolution in the water column and Si reflux from the sediments.

The profiles of Ca : Sr and DIC during seasonal stratification (Fig. 3) reflect biogenically induced precipitation of

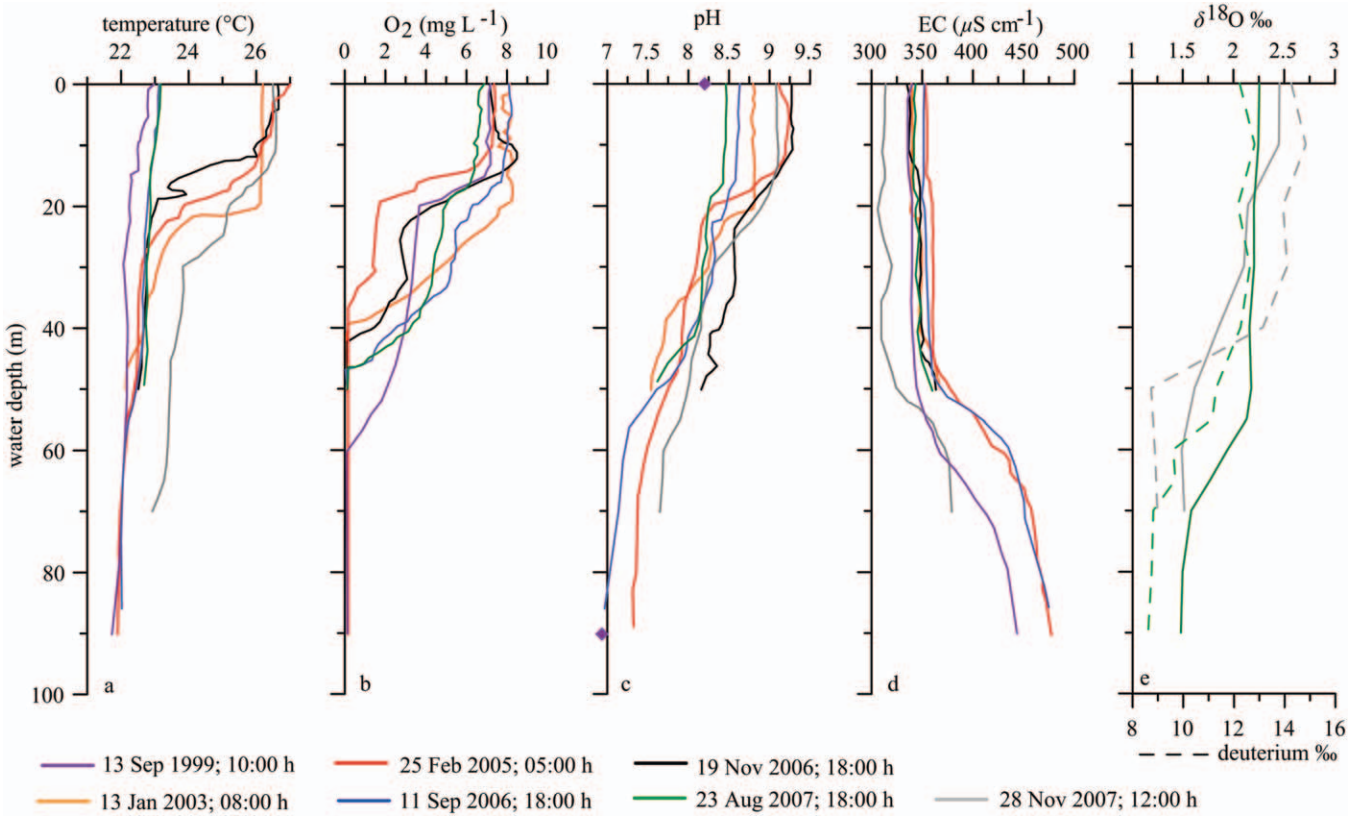

Fig. 4. Temperature, oxygen, pH, EC, and isotope profiles of Lake Challa reflecting seasonal changes in the water stratification and budget between September 1999 and November 2007.

Table 3. Saturation indices of selected minerals with pH and temperature values during an ongoing mixing event (23 Aug 2007) and during stratified conditions (28 Nov 2007).

			SI		
Depth (m)	Temp(°C)	pH	Calcite	Aragonite	Si(a)
23 Aug 2007					
0	23	8.5	0.58	0.43	−0.42
10	23.1	8.5	0.59	0.44	−0.42
20	22.9	8.25	0.34	0.2	−0.41
30	22.7*	8.2*	0.32	0.17	−0.41
40	22.5	8.1	0.22	0.07	−0.4
50	22.3*	7.7*	−0.08	−0.23	−0.38
60	22.1	7.25	−0.35	−0.49	−0.32
70	22.05*	7.12*	−0.37	−0.52	−0.26
80	22	7	−0.47	−0.61	−0.26
28 Nov 2007					
0	26.5	9.1	1.15	1.01	−0.5
10	26.4	9.1	1.15	1	−0.48
20	26.5	9.1	1.13	0.99	−0.52
40	23.8	8.25	0.42	0.28	−0.49
60	23.5	7.5	−0.01	−0.22	−0.31
80	23.4*	7.5*	−0.3	−0.44	−0.41
90†	23.2*	7.5*	−0.29	−0.44	−0.41
95	23	7.5	−0.3	−0.44	−0.4

* pH and temperature values interpolated.
† Average of two water analyses, Si(a) amorphous silica, hydrochemical data for Phreeq-calculations of saturation indices (SI) *see* Table 1.

low-Sr $CaCO_3$, driven by biogenic uptake of CO_2 in the euphotic zone, dissolution of settling autochthonous carbonate particles in water depths > 40 m, and Ca reflux across the sediment–water interface. An oversaturation increase of calcite in the upper 40 m of the water column was recorded from 23 August to 28 November 2007 (Table 3).

Very low Fe and Mn concentrations, down to 40 m water depth in August 2007 and in the whole water column (except at ~ 60 m and 95 m) in November 2007 (Fig. 3c,i), reflect the precipitation of Fe(Mn)OOH in oxygenated water. Increasing Fe and Mn concentrations downward from the upper hypolimnion in August 2007 document the diffusive reflux of Fe and Mn from the surface sediments, which is sustained by the microbe-mediated reduction of reactive Fe(Mn)OOH and Fe(Mn)-release into the pore water of the sediments. The greater increase of Mn in comparison to Fe (Mn : Fe maximum at ~ 50 m water depth; Fig. 3b) indicates that prevailing pH–Eh conditions favored the precipitation of dissolved Fe or the release of Mn^{2+} from settling Fe(Mn)OOH precipitates and from the sediments (excluding subsurface inflow with high Mn : Fe ratios) or both.

Compared to other African stratified lakes (Talling 1966; Davison 1993), Fe concentrations in the anoxic hypolimnion of Lake Challa (in August 2007) are relatively low. Profiles from 28 November 2007 document the chemical stratification shortly after overturn. The deep-water concentrations

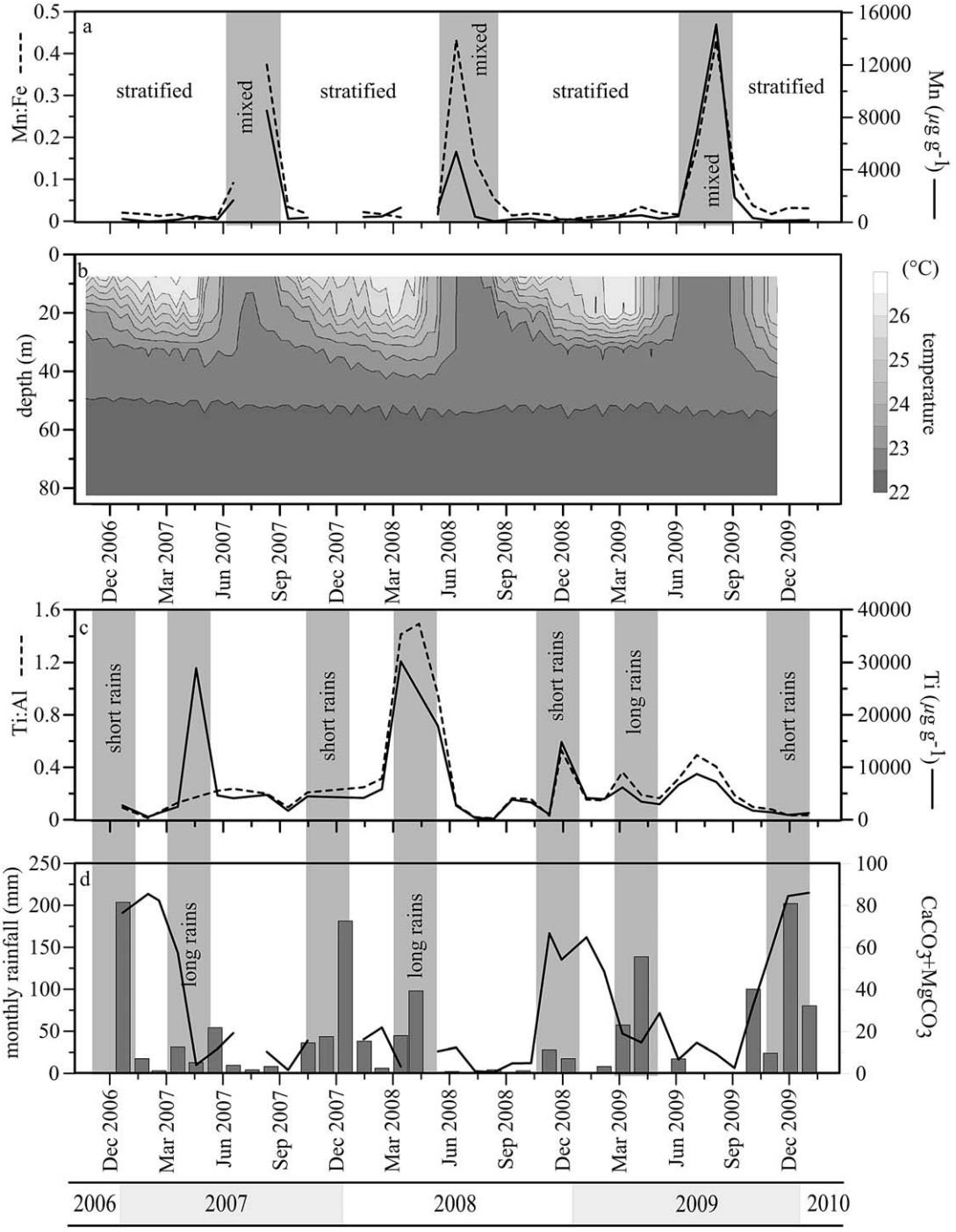

Fig. 5. Selected data for changes in the composition of sediment trap materials in the context of seasonal meteorology and changes in water-column stratification. (a) Mn : Fe ratios and Mn contents; shaded bars mark the seasonal overturn. (b) Seasonal changes in water-column stratification on temperature records received from thermistor data. (c) Ti contents and Ti : Al ratios of sediment trap materials; increase in Ti : Al marks higher proportions of siliciclastic input of local provenance. (d) Carbonate contents of sediment trap materials calculated as $CaCO_3$ on the basis of TIC analyses (solid line) and monthly rainfall data from the meteorological station in Voi (Kenya) (bars).

of Fe^{2+} and Mn^{2+} certainly increased during the stratification period until their seasonal precipitation.

With TDS concentrations of approximately 350 mg L^{-1} (Table 1), the water of the mixed Lake Challa is moderately mineralized (Talling and Talling 1965). The salinity of the lake was fairly constant between September 1999 and November 2007 (Fig. 4d). The maximum EC variation in the upper 45 m of the water column ($\sim$ 25 μS cm^{-1}) may largely depend on interannual variations in the lake water overturn and calcite precipitation. The current TDS of

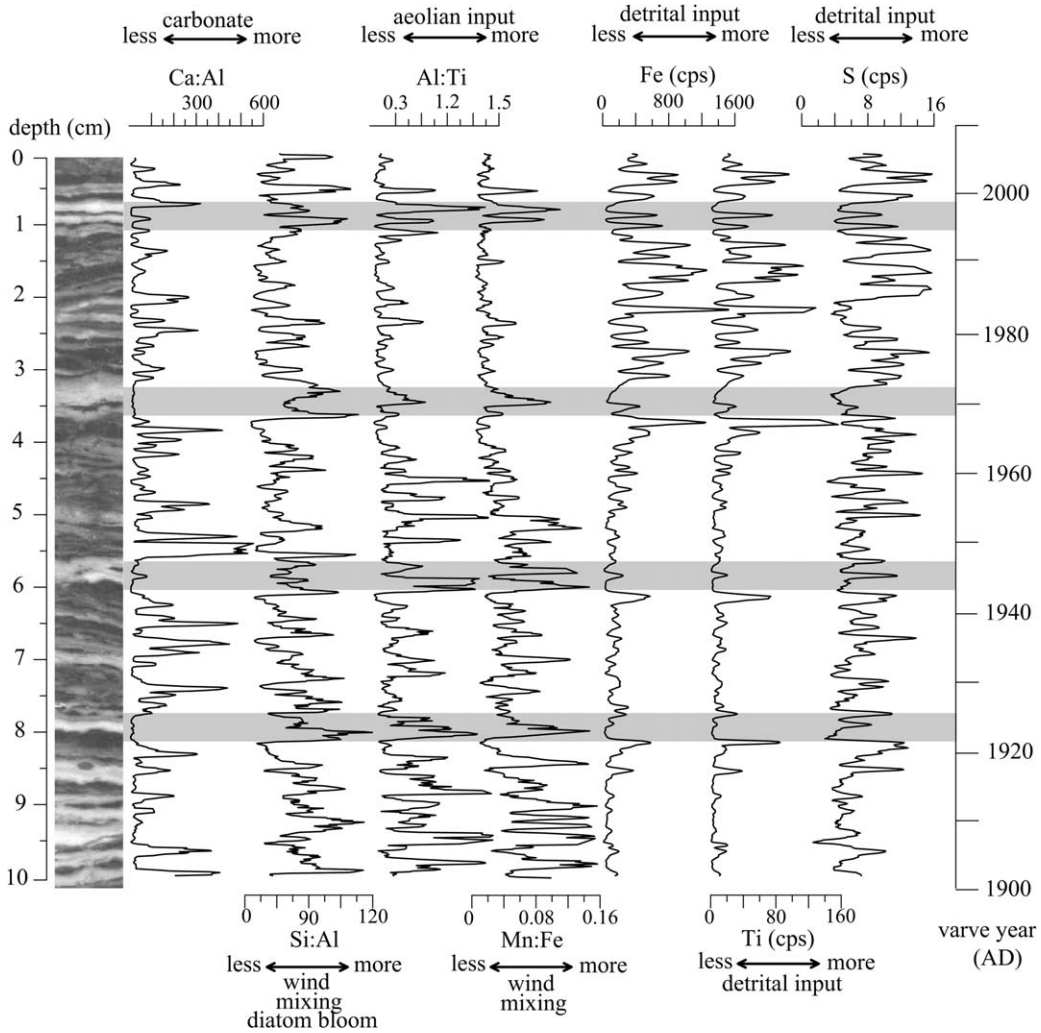

Fig. 6. Selected μXRF profiles of a thin section block from short core CH05-1G (0–10 cm depth). Curves represent five-point running averages; gray bars mark prominent diatom laminae. Chronology of counting varves is linked to and consistent with absolute calendar timescale using the existing age model (Blaauw et al. 2011) based on ^{210}Pb and ^{14}C dating (supporting online material in Wolff et al. 2011).

Lake Challa may have been built up over a long period by evaporative enrichment.

Thermal and chemical stratification—Limnological surveys conducted between September 1999 and November 2007, in combination with meteorological monitoring data from Voi (Kenya) (Fig. 2; ~ 100 km to the east of Lake Challa), were used to interpret seasonal changes in the thermal and chemical stratification of Lake Challa. The seasonal formation of a well-defined thermocline is related to warming during the southern hemisphere winter (October–May) and generally low wind stress during this season. The thermal stratification of the water column is not sustained year-round, due to cooling and intensified wind during the dry season. Our monitoring data imply a yearly minimum turnover of the upper 45 m of the lake (Fig. 5b), with reduced vertical temperature gradients during the southern hemisphere winter (Figs. 4a, 5b). Temperature and oxygen profiles document distinct interannual variations in the intensity of seasonal mixing events, depending on cooling and wind stress during the year (Figs. 4b, 5b). There is, however, no simple correlation between water-column mixing and the penetration depth of O_2. The advective and diffusive downward flux of O_2 is additionally determined by the diurnal production and consumption of O_2 by phytoplankton and by microbe-mediated organic matter degradation.

The increase in EC and TDS between ~ 45 m and 60 m of the water profile from 23 August 2007 suggests that seasonal mixing was limited to a water depth of ~ 50 m (Fig. 4d; Table 1). The undisturbed finely laminated pattern of the sediments (Fig. 6) indicates that the lake bottom was seasonally anoxic over longer periods, which is supported by the oxygen profiles (Fig. 4b).

The O_2 profile in November 2006 exhibits maximum O_2 concentrations at ~ 10 to 15 m, whereas in all other profiles O_2 concentrations are constant (or decrease with depth) within the upper ~ 15 m (Fig. 4). Such maxima commonly

Table 4. Chemical composition of sediment trap samples.

Date	Sample description*			TOC	$CaCO_3$†	Silicon‡	Ti	Al	Fe	Mn	Mg	Ca
	Calcite	Organic	Diatoms		(%)		(μg g^{-1})					
30 Dec 2006	x			7.0	76.5	36	2716	29,624	12,214	250	18,469	280,339
10 Feb 2007	x			6.0	85.6	50	530	40,945	2673	44	15,245	320,964
28 Feb 2007	x			6.3	82.4	27	1288	22,020	6794	86	16,339	306,882
31 Mar 2007	x			15	57.4	23	2469	18,878	12,111	205	12,463	212,233
30 Apr 2007		x		23	NA	NA	NA	NA	NA	NA	NA	NA
04 Jun 2007		x	x	31	11.8	26	4633	20,974	19,913	221	8952	34,524
30 Jun 2007		x	x	27	19.2	21	4092	17,308	18,319	1675	9029	64,292
31 Jul 2007		x		28	NA	NA	NA	NA	NA	NA	NA	NA
24 Aug 2007			x	DL	10.4	29	4731	23,787	22,815	8515	8390	29,823
28 Sep 2007			x	11	1.7	22	1706	17,921	7742	263	2264	3792
30 Oct 2007			x	17	15.6	26	4448	21,317	20,028	346	11,266	46,818
01 Dec 2007	x			NA	NA	NA	NA	NA	NA	NA	NA	NA
31 Dec 2007	x			20	NA	NA	NA	NA	NA	NA	NA	NA
30 Jan 2008	x			21	16.2	20	4142	16,719	18,389	401	7895	53,871
29 Feb 2008		x	x	17	21.9	23	5834	18,580	26,167	442	10,002	73,528
31 Mar 2008		x	x	2.7	3.4	26	30,209	21,400	114,902	1114	4886	6718
30 Apr 2008		x		3.0	4.2	24	28,908	19,372	102,416	465	4943	9844
31 May 2008		x	x	11	10.6	23	17,872	18,733	65,363	1096	8563	30,367
30 Jun 2008		x	x	7.7	12.4	29	2681	23,440	12,421	5377	5207	42,336
31 Jul 2008		x	x	5.0	1.2	22	342	17,678	2947	425	1525	2605
31 Aug 2008			x	4.9	0.7	21	177	17,181	1491	81	761	1573
30 Sep 2008			x	5.7	4.9	29	3829	23,446	16,472	227	7351	9397
31 Oct 2008			x	10	5.0	26	3295	21,040	14,467	269	4740	13,372
30 Nov 2008	x		x	7.5	66.9	40	1010	33,247	4601	70	9808	253,670
20 Dec 2008	x			9.1	54.3	34	14,811	28,041	102,416	221	12,491	199,522
30 Jan 2009	x			8.2	64.9	33	4118	26,821	18,023	171	13,083	241,298
28 Feb 2009	x	x	x	10	48.6	32	3928	26,414	18,173	226	11,549	178,219
30 Mar 2009		x	x	20	19.0	21	6149	16,906	28,250	429	8343	64,195
30 Apr 2009		x	x	25	14.8	22	3431	18,194	15,517	529	5536	51,327
30 May 2009		x	x	26	28.8	22	2951	17,980	13,592	275	8221	103,595
30 Jun 2009	x	x	x	30	6.8	26	6622	21,144	28,809	459	7601	16,430
30 Jul 2009	x	x	x	24	14.6	22	8713	17,690	39,203	6834	10,057	44,376
31 Aug 2009			x	26	9.4	22	7207	17,788	34,978	15,090	8894	25,017
30 Sep 2009			x	18	2.7	22	3382	18,031	17,007	1906	3455	5943
30 Oct 2009			x	12	32.0	21	1725	17,591	8628	323	5994	119,717
30 Nov 2009	x		x	8.3	59.6	22	1408	17,797	7013	119	10,189	224,177
27 Dec 2009	x		x	6.1	84.6	32	902	26,531	4113	132	14,451	318,134
30 Jan 2010	x			5.1	86.1	44	1260	35,979	5556	171	16,175	321,879

NA, not analyzed; DL, under detection limit.
* x indicates presence of item.
† $CaCO_3$ = inorganic carbon × 8.33.
‡ Silicon = Al_2O_3 × 100/15.6.

develop in stratified nutrient-limited lakes and reflect enhanced primary productivity around the thermocline (Wetzel 1983). Transparency of surface waters in the stratified Lake Challa is high (Secchi depth of 5 to 7 m; Damsté et al. 2009).

Stable isotope profiles for August and November 2007 provide information about the water budget and seasonal mixing of the water column (Fig. 4e). The August 2007 data show that seasonal mixing did not include the entire water column. The heavier isotope composition of the epilimnion vs. deep water in November 2007 indicates seasonal evaporative enrichment of Lake Challa. The $\delta^{18}O$ data are strongly linked to precipitation and evaporation, with lighter $\delta^{18}O$ caused by precipitation and heavier $\delta^{18}O$ values by an increase in evaporation. The overall heavier isotope composition in Lake Challa vs. precipitation (cf. precipitation Entebbe [Uganda]: average annual $\delta^{18}O$ −2.26‰; average annual deuterium −5.8‰; International Atomic Energy Agency 1992) has been adjusted over longer timescales. At multiannual scales, paleo-$\delta^{18}O$ data for Lake Challa were inferred from a diatom isotope study and reflect the aggregated balance between the amount of precipitation and the intensity and duration of dry-season evaporation (Barker et al. 2011).

The detrital allochthonous sediment fraction—The siliciclastic sediment fraction comprises the input of local soil particles by surface run-off from a restricted area and aeolian influx of a wider source region. Table 2 compiles the bulk chemical composition of various representative materials from around Lake Challa. Local soils and their basic precursor rocks have much higher Fe, Mg, Ti, Ca,

Table 4. Extended.

Sr	Na	K	La	Y	P	S						
			(μg g^{-1})				Ca : Sr	Al : Fe	Ca : Al	Fe : Al	Al : Ti	TOC : P molar
846	993	1533	DL	3	1953	2127	332	2.4	9.5	0.41	10.9	92.6
834	373	446	1	2	3692	1471	385	15.3	7.8	0.07	77.2	41.8
835	582	816	4	2	905	1579	368	3.2	13.9	0.31	17.1	181.0
605	544	1784	10	6	2248	3530	351	1.6	11.2	0.64	7.6	173.9
NA	NA	NA	NA	NA	NA	NA						
258	1455	2788	19	7	4106	7503	134	1.1	1.6	0.95	4.5	195.6
339	766	2388	15	5	5124	7625	189	0.9	3.7	1.06	4.2	137.8
NA	NA	NA	NA	NA	NA	NA						
214	2146	2825	15	5	5870	4294	139	1.0	1.3	0.96	5.0	
44	415	1001	5	2	2584	3544	87	2.3	0.2	0.43	10.5	106.8
430	2397	4654	18	6	5302	7345	109	1.1	2.2	0.94	4.8	83.6
NA	NA	NA	NA	NA	NA	NA						
NA	NA	NA	NA	NA	NA	NA						
502	1496	3764	18	6	4426	7506	107	0.9	3.2	1.10	4.0	123.6
524	1453	3861	23	10	4576	6857	140	0.7	4.0	1.41	3.2	94.6
123	743	3552	123	41	7677	1075	54	0.2	0.3	5.37	0.7	9.0
147	556	3181	122	38	5984	1011	67	0.2	0.5	5.29	0.7	12.9
263	3511	6997	75	26	6591	5764	116	0.3	1.6	3.49	1.0	44.7
179	394	1233	13	5	2593	2928	236	1.9	1.8	0.53	8.7	76.8
27	721	651	2	1	2077	2852	97	6.0	0.1	0.17	51.6	62.5
13	201	230	1	1	1124	2345	117	11.5	0.1	0.09	96.8	113.1
150	810	1468	10	4	1639	2617	63	1.4	0.4	0.70	6.1	89.7
133	824	1917	12	4	2239	3205	100	1.5	0.6	0.69	6.4	116.3
620	332	503	4	3	899	1074	409	7.2	7.6	0.14	32.9	215.1
601	873	2591	60	20	3793	1955	332	0.3	7.1	3.65	1.9	61.9
670	713	1951	DL	7	2108	2305	360	1.5	9.0	0.67	6.5	100.3
649	1161	2231	DL	6	1711	2325	274	1.5	6.7	0.69	6.7	152.3
272	1183	3682	23	9	2411	4696	236	0.6	3.8	1.67	2.7	210.7
282	896	1950	10	5	2567	5083	182	1.2	2.8	0.85	5.3	250.1
526	1051	2028	8	5	2679	6658	197	1.3	5.8	0.76	6.1	248.3
178	1318	3123	25	8	4372	8308	92	0.7	0.8	1.36	3.2	176.3
318	1657	3762	34	11	12,045	7755	139	0.5	2.5	2.22	2.0	50.5
234	1609	3688	29	10	6404	9837	107	0.5	1.4	1.97	2.5	103.1
70	738	1956	12	5	3200	5272	85	1.1	0.3	0.94	5.3	144.3
304	518	1201	8	4	1937	3353	394	2.0	6.8	0.49	10.2	159.8
517	464	1056	6	3	1308	2233	434	2.5	12.6	0.39	12.6	163.6
726	355	519	3	2	2273	1444	438	6.5	12.0	0.16	29.4	69.2
711	367	873	4	3	2256	1206	453	6.5	8.9	0.15	28.6	58.3

and P than acidic gneisses of the basement, which outcrops at some distance from the lake (Table 2). Dust influx of remote provenance, if contributing in substantial amounts to the bulk siliciclastic influx, may be characterized by geochemical signatures similar to mean Upper Continental Crust (UCC) composition (Rudnick and Gao 2003).

Sediment trap samples—Optical and electron microscopy of sediment trap samples reveal three major components: (1) autochthonous calcite, predominantly precipitated during southern hemisphere summer, (2) amorphous organic and fine-grained (clay-sized) siliciclastic matter settling during the long rainy season, and (3) diatoms mainly deposited during the southern hemisphere winter period (Table 4). The percentage of siliciclastic matter in the trap materials is estimated on the basis of ICP-AES analyses, assuming a constant Al_2O_3 concentration of the inorganic detrital influx (15.6 wt%, mean continental crust composition; Taylor 1964). On this basis the siliciclastic matter in the traps ranged between 20.3 wt% and 49.6 wt% (average: 26.7 wt%, SD 7.0). Values above 30% are only recorded during the rainy seasons between November and March. The Al : Ti mass ratio of most samples is rather low (minimum 0.7, average 14) as expected for input of local rock particles of basaltic composition (average basalt 11.0; Taylor 1964). However, six trap samples show distinctly higher Al : Ti (29–97) and lower Fe : Al ratios (0.07–0.17), probably representing a second siliciclastic component. Siliciclastic matter of remote provenance is delivered by aeolian input and contributes to the detrital sedimentary component. The highest Al : Ti ratio was determined for material collected in August 2008 during the dry and windy season (Table 4).

Seasonal changes between oxic and anoxic conditions lead to enrichment and depletion of dissolved Fe and Mn in the hypolimnion (Balistrieri et al. 1994; Schettler and

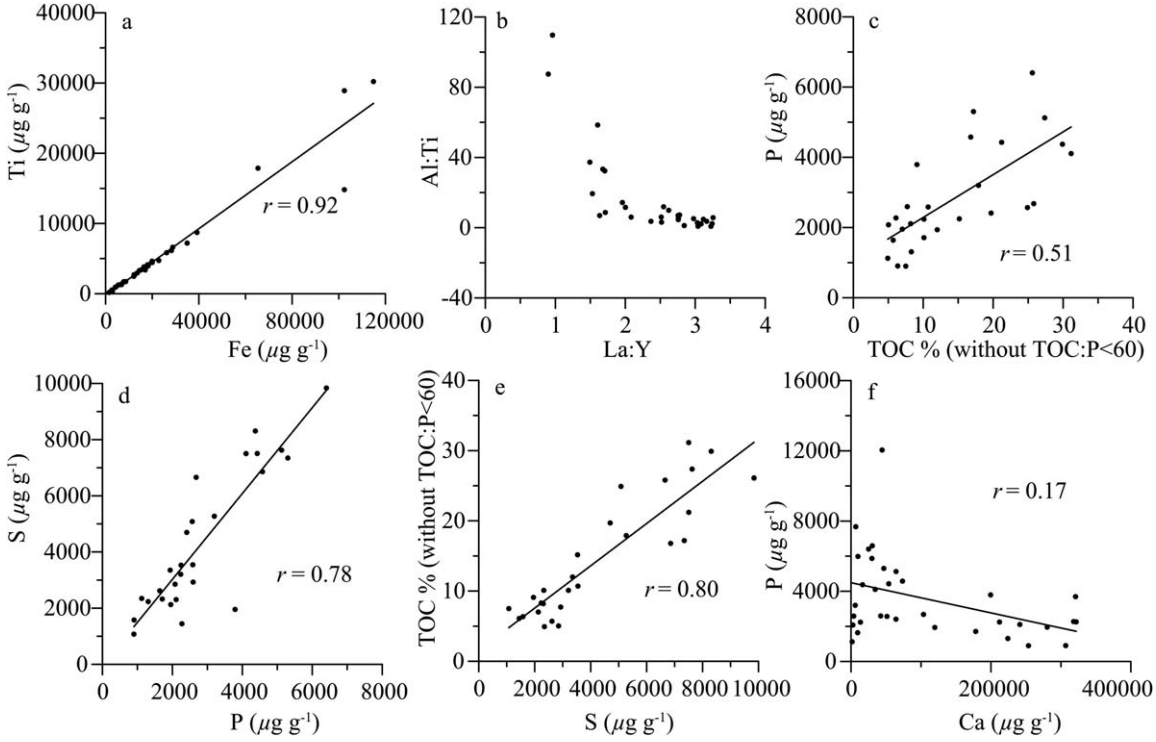

Fig. 7. Chemical data of sediment trap materials collected between 2006 and 2010. (a) Ti vs. Fe, reflecting that the input of both major elements largely relates to detrital influx; changing contributions from local debris and dust of remote provenance does not much affect the correlation because variations in the portion of the local Fe- and Ti-rich components likewise affect the concentration of both elements in the trapped sample. (b) Al : Ti vs. La : Y, local trachy-basalts are relatively enriched in TiO_2 and La vs. dust of remote provenance. The horizontal trend in the diagram relates to samples with high contributions from local siliciclastics and reflects variable enrichment of La in the local volcanic rock types. The positive offset from the horizontal trend represents samples with higher contributions from dust. (c) P vs. TOC, the P contents are largely organically bound; the intercept with the P-axis at ca. 1000 $\mu g\ g^{-1}$ reflects P bound to the inorganic detrital influx and chemically precipitated dissolved P from the lake water. (d, e) Correlation diagrams of S vs. P and TOC vs. S. (f) Correlation diagram of P vs. Ca; the weak inverse correlation does not support sorption of PO_4 on settling calcite crystals to be a significant controlling factor for the abiotic removal of dissolved P from the lake water.

Albéric 2008). The hydrochemical composition of the groundwater input (no data available), the diffusive reflux of Fe and Mn from the sediments, and the pH–Eh conditions in the hypolimnion cause seasonal enrichment of Mn^{2+} vs. Fe^{2+} in the deep water of Lake Challa (Fig. 5). Seasonal overturn events oxygenate the deep water, causing precipitation of Fe : MnOOH and, consequently, high Mn and Mn : Fe ratios in sediment trap materials (Fig. 5).

Monthly Ca varies substantially, from 0.2 wt% to 32.2 wt%, reflecting distinct seasonal variation in the precipitation of autochthonous calcite (cf. microscopic component analyses, Table 4). Highest $CaCO_3$ occurred between November and March in the short rainy season. A positive correlation between $CaCO_3$ and Ca : Sr ($R^2 = 0.78$; $n = 33$) indicates that autochthonous $CaCO_3$ is a low-Sr component (cf. Ca : Sr water profile; Fig. 3).

Total P in the sediment trap samples comprises (1) organically bound P of planktonic matter, (2) dissolved PO_4 removed by chemical (co-)precipitation or sorption on settling inorganic particles, and (3) P associated with the allochthonous detrital organic and inorganic input. The monthly molar TOC : P ratios of the trap material vary between 9.0 and 250.1 (average 119), showing major positive and negative deviations from the Redfield ratio (C : P = 106 : 1; Redfield 1958). In our interpretation, TOC : P values distinctly below 106 indicate substantial P contributions from abiotic nonplanktonic components. P and TOC positively correlate ($R^2 = 0.51$) with excess P, if samples with TOC : P < 60 are not considered (Fig. 7).

The same trap samples also show a positive correlation with sulfur ($R^2 = 0.80$), indicating that most sulfur is bound to organic matter (Fig. 7). Ca shows no positive correlation with P. Therefore, sorption of PO_4 onto settling calcite crystals can be rejected as a significant controlling factor for the abiotic removal of PO_4 from the water. Relative changes in the abundance of diatoms in trap materials, estimated on the basis of microscopic smear-slide inspection and SEM analyses (Table 4), document that diatoms were highest between June and September.

Sediments—In 2005, a 20.81 m long continuous core spanning the past 25,000 yr was recovered from the center of Lake Challa. The sediment profile is dominated by sequences of fine light–dark couplets, the same as those found in the uppermost 10 cm of the short gravity core (CH05-1G). The chronology of the long sediment profile

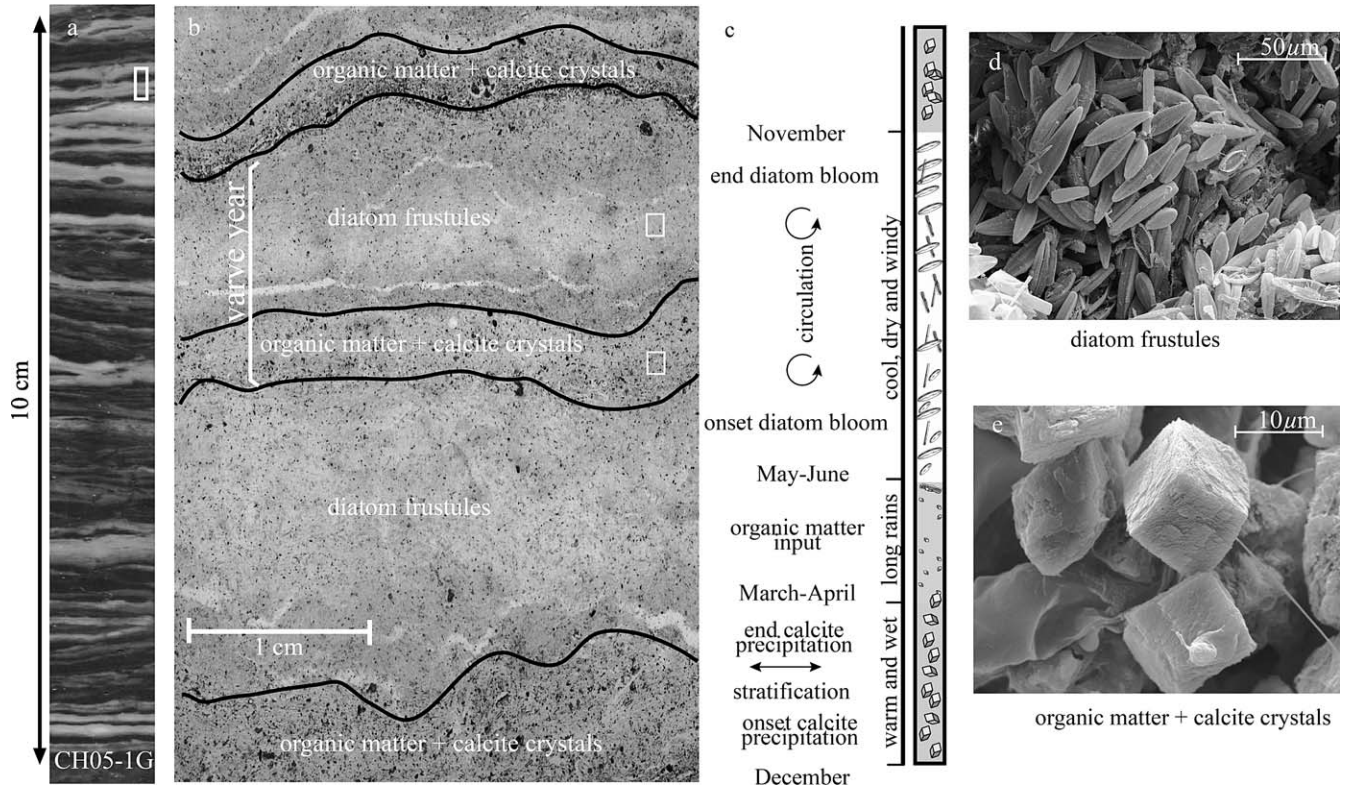

Fig. 8. (a) Photograph of laminated sediments of core CH05-1G, showing the succession of light and dark layers. (b) Microfacies analysis reveals that the dark layers predominantly consist of amorphous organic matter and crystals of autochthonous calcite. Diatom frustules are the overall dominant constituents of the light layer. (c) Establishment of a varve model and annual sedimentation within Lake Challa—with the darker layer representing the warm and wet southern hemisphere summer and the light layer the cool, dry, and windy southern hemisphere winter period. (d) SEM photograph of a light lamina with planktonic diatom content (*Gomphocymbella* sp.). (e) SEM image of calcite crystals imbedded in the dark layer.

is based on 168 AMS ^{14}C dates and ^{210}Pb dating (Verschuren et al. 2009; Blaauw et al. 2011). Radiometric dating and analysis of the monthly collected sediment trap material confirmed that the light–dark couplets record annual deposition (supplement in Wolff et al. 2011). Based on microscopic inspection, the dark layers are mainly composed of amorphous organic matter and fine-grained siliciclastics, with single silt-sized calcite crystals imbedded in this matrix. Diatom skeletons (*Gomphocymbella* sp. and *Nitzschia* sp.) are the dominant constituents of the light layers (Fig. 8; Barker et al. 2011; Barker et al. 2013).

The chronology for the upper 10 cm of core CH05-1G was established by counting the light–dark couplets representing the past 100 ± 2 yr. This floating chronology was linked to the absolute timescale of the existing 25,000 yr chronology of the long core, using distinct marker layers. In lacustrine environments such varve types are classified as carbonaceous organic varves (Zolitschka 2007). Varved sequences potentially provide information about past environmental changes by variations in structure, composition, and thickness (Ojala et al. 2012).

Investigation of annually laminated lake sediments with μXRF scanning provides additional information on seasonal signals and long-term changes (Yancheva et al. 2007; Brauer et al. 2008). The μXRF scans, applied on a 10 cm resin block of core CH05-1G, show Ti and Fe maxima and Si : Al minima for the dark laminae, and the light diatom-rich layers show Si : Al maxima and Fe and Ti minima (Fig. 6). Ca : Al maxima occurring within the dark layers document seasonally enhanced deposition of autochthonous calcite. Light layers, documenting seasonal diatom blooms (Si : Al maxima), coincide with Mn, Mn : Fe, and Mn : Ti maxima that indicate chemical precipitation of Mn during overturn events (Figs. 5, 6).

In local rocks and soils, the concentration of Fe is approximately 70 times higher than the Mn concentration. Therefore, variations in the Fe : Ti and Fe : Al ratios document the chemical precipitation of dissolved Fe (with a low sensitivity compared to Mn ratios) or uncertainty due to the different chemical composition of detrital influx of local and remote provenance. Count ratios of Al : Ti calculated from μXRF scans display peaks in the light laminae. Al : Ti maxima indicate the influx of Al-rich siliciclastic matter of remote provenance during the windy and dry season. Total sulfur is clearly enriched in the dark layers (Fig. 6) and is related to organically bound S and/or Fe-sulfide.

The use of Ti for normalization probably overestimates the portion of chemically precipitated Mn for sediment

sublayers and seasonal trap samples with high contributions from low Ti : Al siliciclastic input of remote provenance, whereas using Al for normalization potentially underestimates the portion of chemically precipitated Mn if high-Ti : Al local detrital input dominates the siliciclastic fraction of sediments and trap materials.

Discussion

Sedimentation model—Sediment trap material confirmed the annual origin of the dark–light couplets in sediment cores. During the windy season (June to October), which coincides with the mixing of the lake, dissolved deep water nutrients become available for phytoplankton growth. Together with the more turbulent water column, these nutrients promote diatom blooms, which are preserved as light layers in the varves (Figs. 6, 8). The darker layers represent the two rainy seasons (November to December and March to May) and the brief intervening dry season with amorphous organic matter derived from phytoplankton and calcite precipitation.

The influx of local siliciclastics is dominated by local basaltic debris during the combined rainy seasons (November–April) washed into the lake by surface runoff. The lake probably also receives dissolved nutrients from surface run-off. Nutrient influx by groundwater inflow depends on rainfall seepage and may also increase as a result of lake-level lowering during the dry season. The influx of N and P is hardly detectable in lake water because it is immediately consumed by phytoplankton. During the rainy season, calcite oversaturation increased in the upper 20 m of the water column (Table 3). Seasonal biogenically induced precipitation of low-Sr calcite crystals is well documented by the water profiles of Ca and DIC, as well as Ca : Sr ratios of monthly trap data and the composition of calcareous organic-rich layers in the sediment.

Diatom growth is strongly limited by SRP in the stratified lake. Partial overturn of the water column is related to an increase of local wind stress and cooling during the dry season (May–October). The internal nutrient cycle supports seasonal diatom blooms, particularly by vertical advective transport of SRP into the euphotic zone. Hydrochemical data during the overturn period in August 2007 show undersaturation of calcite in contrast to stratified conditions in November 2007 (Table 3). During the dry seasons between 2006 and 2009, calcite contents were distinctly lower or were even completely absent in the monthly trap material (Table 1).

The 100-yr sediment record documents the regular seasonal presence of light-colored noncalcareous diatom-rich layers. The decline or even absence of seasonal calcite precipitation is associated with a number of factors: (1) calcite precipitation in the previous season, (2) temperature decrease, (3) mixing with CO_2-rich deep water buffering the pH increase associated with the CO_2 uptake by phytoplankton, and (4) possible kinetic inhibition of crystal growth by PO_4 (Dittrich and Koschel 2002) or the composition of Mg–calcite cements influenced by the Mg : Ca ratio of the solution from which they precipitated (Mucci and Morse 1983; Morse and Mackenzie 1990).

The intensity, duration, and timing of the onset of vertical mixing of the water column are annually variable. During the period of seasonal stratification, dissolved Fe and Mn are enriched in the anoxic deep water and precipitate by oxygenation of the deep water during overturn events. The net accumulation of chemically precipitated Mn in the sediment distinctly exceeds that of Fe due to hydrochemical characteristics of the groundwater inflow and prevailing pH–Eh conditions or both. The chemical precipitation of Mn is sensitively recorded in μXRF scans of the sediments by Mn : Ti(Al) and Mn : Fe maxima that coincide with light diatom-rich laminae deposited during overturn events in the dry season. Chemical characteristics of monthly trap materials demonstrate that the siliciclastic influx comprises a local (basaltic) component and a remote component characterized by high Al : Ti and by a La : Y mass ratio close to 1. The ratio of both end members in the depositional flux shows seasonal variability. Siliciclastic matter deposited during the dry and windy season occurring in the light layer is clearly enriched in the high Al : Ti component and reflects aeolian input.

The climate archive of Lake Challa—Lake hydrology reconstructions of the past 25,000 yr show that the lowermost water column remained stratified and created anoxic conditions at the sediment–water interface, which promotes preservation of the seasonal laminae (Moernaut et al. 2010; Barker et al. 2013). Biogenic silica resulting from diatom blooms in the dry season is a major sediment component of the Lake Challa sediments over the last 25,000 yr (biogenic silica range 20–70%; Barker et al. 2011, 2013). These blooms are associated with overturn events, which positively correlate with the internal P cycle during overturn, and are quantifiable by the thickness of the light diatom layers. Seasonal upwelling of the deep-water SRP reservoir strongly depends on wind strength and temperature decrease during the dry season; therefore, the net accumulation of biogenic opal (varve thickness and percentages of biogenic silica) can be used as a proxy to reconstruct paleo wind variations during the dry season (Wolff et al. 2011; Barker et al. 2013). Assuming that present-day associations between El Niño dynamics (wetter [drier during La Niña] and decreased [increased during La Niña] wind speeds) in East Africa existed throughout the period recorded in our long core, we can interpret the Lake Challa sediments as indicating that thick varves represent windier La Niña conditions and that thinner varves are El Niño indicators. Variations in varve thickness (between 0.08 and 7 mm yr^{-1}) thus show evidence for interannual to centennial-scale changes in ENSO-related rainfall variability over the past 25,000 yr (Wolff et al. 2011).

Photosynthetic production in the lake is strongly limited by SRP availability. Accumulation of SRP in the deep water depends on (1) external influx (mainly groundwater inflow), (2) SRP removal during previous overturn events, and (3) SRP flux from the surface sediments across the sediment–water interface. The latter has to be considered for paleoclimatic interpretations.

Al : Ti and La : Y may be additional suitable climate proxies for local wind strength and mixing of the water column. Increase of Al : Ti and decrease of La : Y potentially

record enhanced aeolian influx of remote provenance related to changes in the wind regime and the dryness in the source region of the dust, or both. Wind-induced mixing leads to higher Mn : Fe (Mn : Ti) and Si : Al ratios. The similar trend of Al : Ti illustrates the link between the external signal via dust and the internal lake response via mixing. Both ratios combined produce a reliable proxy for wind strength.

Limnological surveys conducted between September 1999 and November 2007 document seasonal variability in the sediment formation of Lake Challa, which is in agreement with meteorological observations in this region. During the generally warmer southern hemisphere summer months (October–May), stable thermal water stratification develops, and nutrient inflow during these rainy months supports peak photosynthetic activity in the euphotic zone. During southern hemisphere winter months (June–September), the vertical temperature gradient decreases strongly and southeasterly trade winds cause a pronounced thickening of the mixed layer, which varies from year to year. Deep and continuous mixing permits enhanced blooming of diatoms.

Based on lake water analyses, results from sediment trap analyses, and geochemical investigations on laminated sediments, we developed a model for the formation of laminated sediments in Lake Challa that is in good agreement with the observed seasonal changes in limnology and regional meteorological conditions. We show that diatom blooms are related to deeper mixing in the lake, which is documented by high Mn : Fe ratios within the light diatom-rich sediment laminae and in the sediment trap samples. Simultaneously, high Al : Ti ratios document enhanced aeolian influx of remote provenance. Dark laminae are characterized by higher detrital influx and, therefore, high Fe, Ti, and S concentrations. Low Mn : Fe ratios and observations of Fe-sulfides in dark laminae suggest strongly reducing conditions at the lake bottom during well-stratified periods. Sedimentological and geochemical investigations of recent sediments document a distinct seasonality in the record, and results from ongoing lake monitoring will probably allow even finer differentiation of these signals. These results from the Lake Challa sediment archive identify the site as a highly valuable target for high-resolution paleoclimate studies in East Africa.

Acknowledgments

This work has received funding from the European Science Foundation Collaborative Research (ESF-EUROCORES) program EuroClimate (Climate variability and past, present, and future carbon cycle), project CRP28-CHALLACEA (Lake Challa: A long archive of climate in Equatorial Africa), and Graduate School 1364 Shaping Earth's Surface in a Variable Environment funded by the Deutsche Forschungsgemeinschaft (DFG). Christian Wolff is also grateful for a grant from Leibniz Center for Earth Surface Process and Climate Studies. Fieldwork was conducted with research permission of the Kenyan Ministry of Education, Science and Technology (MOEST) to Dirk Verschuren (13/001/11C). We further acknowledge Jasper Moernaut for the bathymetric map, and Ursula Kegel for laboratory support. Caxton Mukhwana Oluseno is especially thanked for his unfailing lake monitoring work and, finally, all the Kenya crew members without whose assistance in transport, surveillance, and accommodation this project could not have been done. We are grateful to two anonymous reviewers.

References

Balistrieri, L. S., J. W. Murray, and B. Paul. 1994. The geochemical cycling of trace-elements in a biogenic meromictic lake. Geochim. Cosmochim. Acta **58:** 3993–4008, doi:10.1016/0016-7037(94)90262-3

Barker, P. A., E. R. Hurrell, M. J. Leng, C. Wolff, C. Cocquyt, H. J. Sloane, and D. Verschuren. 2011. Seasonality in equatorial climate over the past 25 k.y. revealed by oxygen isotope records from Mount Kilimanjaro. Geology **39:** 1111–1114, doi:10.1130/G32419.1

———, and others. 2013. Carbon cycling within an East African lake revealed by the carbon isotope composition of diatom silica: A 25-ka record from Lake Challa, Mt. Kilimanjaro. Quat. Sci. Rev. **66:** 55–63, doi:10.1016/j.quascirev.2012.07.016

Bear, L. M. 1955. Geology of the Taveta area, explanation of degree sheet 64 N.E. and 64 S.E. *In* Geological survey of Kenya, report no. 32. Nairobi Government Printer.

Blaauw, M., and others. 2011. High-resolution C-14 dating of a 25,000-year lake-sediment record from equatorial East Africa. Quat. Sci. Rev. **30:** 3043–3059, doi:10.1016/j.quascirev.2011.07.014

Black, E., J. Slingo, and K. R. Sperber. 2003. An observational study of the relationship between excessively strong short rains in coastal East Africa and Indian Ocean SST. Mon. Weath. Rev. **131:** 74–94, doi:10.1175/1520-0493(2003)131<0074:AOSOTR>2.0.CO;2

Bluszcz, P., E. Kirilova, A. F. Lotter, C. Ohlendorf, and B. Zolitschka. 2008. Global radiation and onset of stratification as forcing factors of seasonal carbonate and organic matter flux dynamics in a hypertrophic hardwater lake (Sacrower See, northeastern Germany). Aquat. Geochem. **14:** 73–98, doi:10.1007/s10498-008-9026-3

Brauer, A., C. Endres, and J. F. W. Negendank. 1999. Late glacial calendar year chronology based on annually laminated sediments from Lake Meerfelder Maar, Germany. Quat. Int. **61:** 17–25, doi:10.1016/S1040-6182(99)00014-2

———, G. H. Haug, P. Dulski, D. M. Sigman, and J. F. W. Negendank. 2008. An abrupt wind shift in western Europe at the onset of the Younger Dryas cold period. Nat. Geosci. **1:** 520–523, doi:10.1038/ngeo263

Buckles, L. K., L. Villanueva, J. W. Weijers, D. Verschuren, and J. S. Damste. 2013. Linking isoprenoidal GDGT membrane lipid distributions with gene abundances of ammonia-oxidizing Thaumarchaeota and uncultured crenarchaeotal groups in the water column of a tropical lake (Lake Challa, East Africa). Environ. Microbiol. **15:** 2445–2462, doi:10.1111/1462-2920.12118

Cullen, N. J., T. Molg, G. Kaser, K. Hussein, K. Steffen, and D. R. Hardy. 2006. Kilimanjaro glaciers: Recent areal extent from satellite data and new interpretation of observed 20th century retreat rates. Geophys. Res. Lett. **33:** L16502, doi:10.1029/2006GL027084

Damsté, J. S. S., J. Ossebaar, B. Abbas, S. Schouten, and D. Verschuren. 2009. Fluxes and distribution of tetraether lipids in an equatorial African lake: Constraints on the application of the TEX86 palaeothermometer and BIT index in lacustrine settings. Geochim. Cosmochim. Acta **73:** 4232–4249, doi:10.1016/j.gca.2009.04.022

Davison, W. 1993. Iron and manganese in lakes. Earth Sci. Rev. **34:** 119–163, doi:10.1016/0012-8252(93)90029-7

Dittrich, M., and R. Koschel. 2002. Interactions between calcite precipitation (natural and artificial) and phosphorus cycle in the hardwater lake. Hydrobiologia **469:** 49–57, doi:10.1023/A:1015571410442

Downie, C., and P. Wilkinson. 1972. The geology of Kilimanjaro. Department of Geology, Univ. of Sheffield.

Eggermont, H., J. Russell, G. Schettler, K. Van Damme, I. Bessems, and D. Verschuren. 2007. Physical and chemical limnology of alpine lakes and pools in the Rwenzori Mountains (Uganda–DR Congo). Hydrobiologia **592:** 151–173, doi:10.1007/s10750-007-0741-3

Gasse, F., V. Ledee, M. Massault, and J.-C. Fontes. 1989. Water-level fluctuations of Lake Tanganyika in phase with oceanic changes during the last glaciation and deglaciation. Nature **342:** 57–59, doi:10.1038/342057a0

Hastenrath, S., D. Polzin, and P. Camberlin. 2004. Exploring the predictability of the "short rains" at the coast of East Africa. Int. J. Climatol. **24:** 1333–1343, doi:10.1002/joc.1070

International Atomic Energy Agency. 1992. Statistical treatment of data on environmental isotopes in precipitation. Technical report no. 331. International Atomic Energy Agency.

Johnson, T. C., E. T. Brown, J. McManus, S. Barry, P. Barker, and F. Gasse. 2002. A high-resolution paleoclimate record spanning the past 25,000 years in southern East Africa. Science **296:** 113–132, doi:10.1126/science.1070057

Kalnay, E., and others. 1996. The NCEP/NCAR 40-year reanalysis project. Bull. Am. Meteorol. Soc. **77:** 437–471, doi:10.1175/1520-0477(1996)077<0437:TNYRP>2.0.CO;2

Mackay, A. W., D. B. Ryves, R. W. Battarbee, R. J. Flower, D. Jewson, P. Rioual, and M. Sturm. 2005. 1000 years of climate variability in central Asia: Assessing the evidence using Lake Baikal (Russia) diatom assemblages and the application of a diatom-inferred model of snow cover on the lake. Glob. Planet. Change **46:** 281–297, doi:10.1016/j.gloplacha.2004.09.021

Merkt, J. 1971. Zuverlässige Auszählungen von Jahresschichten in Seesedimenten mit Hilfe von Groß-Dünnschliffen. Arch. Hydrobiol. **69:** 145–154. [Counting of annual laminations in lake sediments on large thin sections.]

Meyer, H., L. Schonicke, U. Wand, H. W. Hubberten, and H. Friedrichsen. 2000. Isotope studies of hydrogen and oxygen in ground ice-experiences with the equilibration technique. Isotopes Environ. Health Stud. **36:** 133–149, doi:10.1080/10256010008032939

Moernaut, J., D. Verschuren, F. Charlet, I. Kristen, M. Fagot, and M. De Batist. 2010. The seismic-stratigraphic record of lake-level fluctuations in Lake Challa: Hydrological stability and change in equatorial East Africa over the last 140 kyr. Earth Planet. Sci. Lett. **290:** 214–223, doi:10.1016/j.epsl.2009.12.023

Mölg, T., N. J. Cullen, D. R. Hardy, and G. Kaser. 2008. Tropical glaciers, climate change, and society: Focus on Kilimanjaro (East Africa), p. 168–182. *In* B. S. Orlove, E. Wiegandt, and B. H. Luckman [eds.], Darkening peaks: Glacier retreat, science, and society. Univ. of California Press.

Morse, J. W., and F. T. Mackenzie. 1990. Geochemistry of sedimentary carbonates. Elsevier.

Mucci, A., and J. W. Morse. 1983. The incorporation of Mg^{2+} and Sr^{2+} into calcite overgrowths—influences of growth-rate and solution composition. Geochim. Cosmochim. Acta **47:** 217–233, doi:10.1016/0016-7037(83)90135-7

Nicholson, S. E. 2000. The nature of rainfall variability over Africa on time scales of decades to millenia. Glob. Planet. Change **26:** 137–158, doi:10.1016/S0921-8181(00)00040-0

Ojala, A. E. K., P. Francus, B. Zolitschka, M. Besonen, and S. F. Lamoureux. 2012. Characteristics of sedimentary varve chronologies—A review. Quat. Sci. Rev. **43:** 45–60, doi:10.1016/j.quascirev.2012.04.006

Olaka, L. A., E. O. Odada, M. H. Trauth, and D. O. Olago. 2010. The sensitivity of East African rift lakes to climate fluctuations. J. Paleolimnol. **44:** 629–644, doi:10.1007/s10933-010-9442-4

Parkhurst, D. L., and C. A. J. Appelo. 1999. User's guide to PHREEQC (version 2)—a computer program for speciation, batch-reaction, one-dimensional transport, and inverse geochemical calculations. Water-Resour. Invest. Rep. 99-4259. U.S. Geological Survey.

Payne, B. R. 1970. Water balance of Lake Chala and its relation to groundwater from tritium and stable isotope data. J. Hydrol. **11:** 47–58, doi:10.1016/0022-1694(70)90114-9

Petters, S. W. 1991. Regional geology of Africa. Springer-Verlag.

Pilskaln, C. H. 2004. Seasonal and interannual particle export in an African rift valley lake: A 5-yr record from Lake Malawi, southern East Africa. Limnol. Oceanogr. **49:** 964–977, doi:10.4319/lo.2004.49.4.0964

Redfield, A. C. 1958. The biological control of chemical factors in the environment. Am. Sci. **46:** 230A–221.

Ropelewski, C. F., and M. S. Halpert. 1987. Global and regional scale precipitation patterns associated with the El Niño/Southern Oscillation. Mon. Weath. Rev. **115:** 1606–1626, doi:10.1175/1520-0493(1987)115<1606:GARSPP>2.0.CO;2

Rudnick, R. L., and S. Gao. 2003. Composition of the continental crust, p. 1–64. *In* R. L. Rudnick [ed.], The crust, vol. 3. *In* H. D. Holland and K. K. Turekian [eds.], Treatise on geochemistry. Elsevier, doi:10.1016/B0-08-043751-6/03016-4

Schettler, G., and P. Albéric. 2008. Laghi di Monticchio (southern Italy, region Basilicata): Genesis of sediments—a geochemical study. J. Paleolimnol. **40:** 529–556, doi:10.1007/s10933-007-9180-4

Stockhecke, M., F. S. Anselmetti, A. F. Meydan, D. Odermatt, and M. Sturm. 2012. The annual particle cycle in Lake Van (Turkey). Palaeogeogr. Palaeoclimatol. Palaeoecol. **333:** 148–159, doi:10.1016/j.palaeo.2012.03.022

Talling, J. F. 1966. The annual cycle of stratification and phytoplankton growth in Lake Victoria (East Africa). Int. Rev. Ges. Hydrobiol. Hydrograph. **51:** 545–621, doi:10.1002/iroh.19660510402

———, and I. B. Talling. 1965. The chemical compositions of African lake waters. Int. Rev. Ges. Hydrobiol. Hydrograph. **50:** 421–463, doi:10.1002/iroh.19650500307

Taylor, S. R. 1964. Abundance of chemical elements in the continental crust: A new table. Geochim. Cosmochim. Acta **28:** 1273–1285, doi:10.1016/0016-7037(64)90129-2

Verschuren, D., and others. 2009. Half-precessional dynamics of monsoon rainfall near the East African Equator. Nature **462:** 637–641, doi:10.1038/nature08520

Wetzel, R. G. 1983. Limnology. Saunders College Publishing.

Wolff, C., and others. 2011. Reduced interannual rainfall variability in East Africa during the last ice age. Science **333:** 743–747, doi:10.1126/science.1203724

Yancheva, G., and others. 2007. Influence of the intertropical convergence zone on the East Asian monsoon. Nature **445:** 74–77, doi:10.1038/nature05431

Zolitschka, B. 2007. Varved lake sediments, p. 3105–3114. *In* S. A. Elias [ed.], Encyclopedia of quaternary science. Elsevier.

Associate editor: Roland Psenner

Received: 24 July 2013
Accepted: 01 April 2014
Amended: 25 May 2014